https://doi.org/10.17221/106/2021-SWR

The coupling of hillslope- and gully-erosion increases their controlling efforts: A case study in Liaoning Province, China

Xiangguo Fan[1,2], Haoming Fan[1,4], Shuang Dong[3]*

[1]*College of Water Conservancy, Shenyang Agricultural University, Shenyang, Liaoning, P.R. China*
[2]*Tongren University, Tongren, Guizhou, P.R. China*
[3]*Tongren Polytechnic College, Tongren, Guizhou, P.R. China*
[4]*Key Laboratory of Prevention and Control of Soil Erosion and Ecological Restoration in Liaoning Province, Shenyang, Liaoning, P.R. China*

**Corresponding author: fanhaoming@163.com*

Citation: Fan X.G., Fan H.M., Dong S. (2022): The coupling of hillslope- and gully-erosion increases their controlling efforts: A case study in Liaoning Province, China. Soil & Water Res., 17: 123–137.

Abstract: The widespread hillslope- and gully-erosion in Liaoning Province of Northeast China, pose serious challenges to the local agricultural production. Hillslope- and gully-erosion have typically been studied separately; however, there has been little investigation on the relationship of these two types of erosion. In this study, the coupling relationship of the hillslope- and gully-erosion from the perspectives of erosion intensity and land use, as well as the slope gradient, aspect, and shape, was analysed. The study employed remote sensing and geographic information system techniques, and the universal soil loss equation and kriging were used to perform a macroscopic analysis. The results showed that gully-erosion was more severe compared with hillslope-erosion in the study area. The cultivated land has the highest level of human activities, therefore, the most intense hillslope- and gully-erosion. The threshold slope gradients for the hillslope- and gully-erosion are 14° and 6°, respectively. Above the threshold of 6°, the slope gradient is no longer the primary factor affecting the gully-erosion. Sunny slopes have observably more hillslope-erosion than shady slopes, and the highest hillslope-erosion is observed on the south-southeast-facing slopes. The effect of the slope aspect on the gully-erosion should not be ignored, as evidenced by the considerable gully density of the east-northeast-facing slopes which is obviously higher than for slopes with other slope aspects. The highest hillslope-erosion amount and gully density occur on concave slopes, followed by convex and straight slopes, and straight slopes have little effect on the hillslope-erosion, but have a marked impact on the gully-erosion. The results of this work may serve as a scientific reference for the comprehensive control of soil erosion across a slope-gully system in Northeast China.

Keywords: coupling relation; land use; slope gradient, aspect and shape; slope-gully system; soil erosion

Soil erosion is a common problem in agricultural production in developing countries and plays an important role in land degradation, which profoundly impacts political, economic, social, and environmental spheres (Thampapillai & Anderson 1994; Grepperud 1995; Avijit 2018). Globally, approximately 75 billion tonnes of soil are eroded each year, mostly from agricultural land (Dabral et al. 2008). Some of the most severe soil erosion in the world occurs in Asia, at an average annual soil loss rate of 138 t/ha (Anderson & Thampapillai 1990). One of the four largest black soil regions in the world is found

Supported by the National Key R&D Program of China (Project No. 2021YFD1500701) and National Natural Science Foundation of China (Project No. 41371272).

https://doi.org/10.17221/106/2021-SWR

in Northeast China. Liaoning Province partly falls within the black soil region of China's soil and water conservation zoning system, which is an important commodity food production base in China. However, long-term inappropriate land development and unique natural conditions have degraded the black soil resources and resulted in severe soil erosion (Zhang et al. 2016). The black soil thickness of the annual average loss was 0.7–1.0 cm in Northeast China, where the black soil thickness of some areas has been reduced from 80–100 cm at the initial stage of reclamation to 20–30 cm (Shen et al. 2003). The fact that the thickness of the black soil layer is gradually thinning has become an indisputable fact (Liu 2003).

Hillslope-erosion on a large spatial scale is generally evaluated by using the combination of a geographic information system (GIS), remote sensing (RS) and the universal soil loss equation (USLE) model, which has the advantage of cost-effectiveness and high accuracy (Dabral et al. 2008; Xu et al. 2008; Ganasri & Ramesh 2016; Yuan et al. 2016; Anees et al. 2018; Avijit 2018). Rawat et al. (2016) used the USLE model to investigate the risk and risk factors of the soil erosion in the Jhagrabaria watershed. The soil erosion is mild on abandoned land, fallow land, and areas with high vegetation coverage, but high on arable land. Boggs et al. (2001) used the USLE model in conjunction with digital elevation model (DEM) data and land use units to efficiently assess the risk of soil erosion in the Ngarradj watershed in the Jabiru area. Bartsch et al. (2002) used the GIS technique to spatially interpolate parameter sample points from the USLE model to determine the soil erosion intensity of the Camp Williams area in Utah, USA. Land use was found to be the main impact on the spatial variability of the soil erosion risk in the region. Karamage et al. (2016) used the USLE model to predict the intensity of soil erosion in the Nyabarongo River Basin in Rwanda, where terraced farming was found to reduce the soil erosion rate of farmland by 78%. All the aforementioned studies were based on adapting the USLE model to local conditions, with good results.

Field monitoring of gullies commonly involves combining traditional surveying with GIS and global positioning system techniques. The gully morphological characteristics, causes of gully formation, erosion level, and erosion mechanism on small scales can, thus, be determined (Poesen et al. 2003; Hu et al. 2007; Zhang et al. 2007; Wu et al. 2008; Xia et al. 2017; Oparaku & Iwa 2018). The technique of combining RS and GIS is now maturing for use in studying dynamic changes, spatial variations, and in risk assessments of gully-erosion on large scales (Yan et al. 2005; Achten et al. 2008; Conoscenti et al. 2014; Wang et al. 2014, 2017; Al-Abadi et al. 2018; Alireza et al. 2018). For example, Seutloali et al. (2016) assessed gully-erosion along roads in south-eastern South Africa. The slope gradient and road area were found to strongly impact the gully-erosion, compared to the mild influence exerted by the vegetation coverage and precipitation. Jha and Kapat (2009) found dire gully-erosion with significant spatial variation in the Birbhum region of south-eastern West Bengal, India. Aderemi and Iyamu (2012) found that rapidly developing gully-erosion in Ikpoba has resulted in severe land degradation and created a fragile ecosystem. Costa and Bacellar (2007) identified severe gully-erosion in the Velhas watershed area to the northwest of Ouro Preto County in the Sao Francisco Basin, Brazil, where gullies constitute 42% of the total area. Gully-erosion was investigated from different perspectives in these studies to produce valuable conclusions.

Hillslope- and gully-erosion are closely related in terms of the spatial structure and time series involved (Wang et al. 2012). Gully-erosion is a manifestation of severely deteriorating hillslope-erosion. Gully-erosion interacts with hillslope-erosion and forms a vicious circle that continuously exacerbates the soil erosion (Daba et al. 2003; Wang et al. 2014). Slopes and gullies are important parts of watershed systems, which, when investigated separately, cannot elucidate the relationship between the two types of erosion in a watershed. The lack of analysis of this relationship hinders the comprehensive control and management of hillslope- and gully-erosion in watersheds. Therefore, the relationship of hillslope- and gully-erosion is urgently required to solve current problems in soil and water conservation. In this study, RS and GIS techniques were used in conjunction with the USLE model and kriging to compile data on a macro scale. The coupling relationships of the hillslope- and gully-erosion were analysed considering the effect of the erosion intensity and land use, as well as the slope gradient, aspect, and shape. Thus, important soil erosion patterns and rules between the two erosion types were identified. This study provides a theoretical basis for the comprehensive management of soil erosion across a slope-gully system in Northeast China.

https://doi.org/10.17221/106/2021-SWR

MATERIAL AND METHODS

Study area description. Liaoning Province is located in the south of Northeast China (118°53'–125°46'E, 38°43'–43°26'N), with a total land surface area of 1.48 × 10^5 km^2. The Notice on National Soil and Water Conservation Division issued by the General Office of Ministry of Water Resources classifies Liaoning Province into two level-1 divisions: a north-eastern black soil region and a northern rocky mountain area. Liaoning Province borders Hebei Province to the southwest, the Inner Mongolia Autonomous Region to the northwest, Jilin Province to the northeast, and the Korean Peninsula to the southeast across the Yalu River. The jurisdiction of Liaoning Province includes 14 prefecture-level cities and 100 counties (cities and districts) (Figure 1). Liaoning Province is located in a midlatitude region on the eastern coast of Asia and the north-western coast of the Pacific Ocean, which lies within a temperate semi-humid and semi-arid monsoon climate zone. There are four distinctive seasons having a significant intra-year temperature variation, where the annual average temperature of 5–10 °C gradually decreases from the southwest to northeast and from the plains to mountainous areas. The annual average precipitation of 400–1 200 mm gradually decreases from the southeast to northwest, with rainfall from June to August accounting for 60 to 70% of the annual precipitation.

Geo-structurally, Liaoning Province belongs to the North China Craton and consists of three structural units, i.e., the Liaodong Anticline, the Yanshan Subsidence Zone, and the Xiaoliaohe Inland Fault. These units constitute a saddle-shaped landform that has tilted toward the centre from north to south and east to west through geological movement. The East Liaoning and West Liaoning low hills lie to the east and west, respectively, with the vast plains of the lower reach of the Liaohe River in the middle. The mountain, plain, and river cover approximately 8.59 × 10^4, 4.89 × 10^4, 1.33 × 10^4 km^2 of the total area, respectively. The distribution of the soil in Liaoning Province has obvious zonal characteristics. The low hills in eastern Liaoning are mainly a brown soil. The low hills of West Liaoning are also mainly a brown soil, except for the cinnamon soil in Jianping County, Beipiao County, and the northern part of Fumeng County. There is a limited distribution of Aeolian sandy soil in areas bordering Inner Mongolia, such as the north parts of Zhangwu, Kangping, and Changtu Counties. The Panarctic plant flora in Liaoning include north-eastern, North China, and Inner Mongolia steppe flora.

According to China's First National Water Conservancy Survey in 2010, the soil erosion area in Liaoning Province was 4.59 × 10^4 km^2, accounting for 31.4% of its total area, with a water erosion area of 4.40 × 10^4 km^2 and a wind erosion area 0.19 × 10^4 km^2. In addition, 47 193 gullies were distributed in the study area. Therefore, the environmental quality was challenged by soil erosion problems.

Data preparation. This study is based on data collected as part of the fourth census of soil erosion in Liaoning Province of Northeast China. The following basic data were used in this study: thematic GIS data (such as RS, topography, soil, and meteorological data), statistical data, reports, and documents. The RS images and topography data were obtained from panchromatic images acquired by Resources Satellite No. 3 (time course: April–December, 2015; resolution: 2.1 × 2.1 m) and a 1 : 50 000 DEM (resolution: 12.5 × 12.5 m), in which the CGCS2000 national geodetic coordinate system was adopted in the geodetic datum, the 1985 national elevation datum standard was adopted in the elevation datum, and the Gauss-Krüger zonal projection method was adopted for the projection at each scale in 6° zones. The meteorological data included daily precipitation data collected from 39 meteorological stations in four provinces over 55 years: 26 stations in Liaoning Province from 1961 to 2015; five stations in Jilin Province

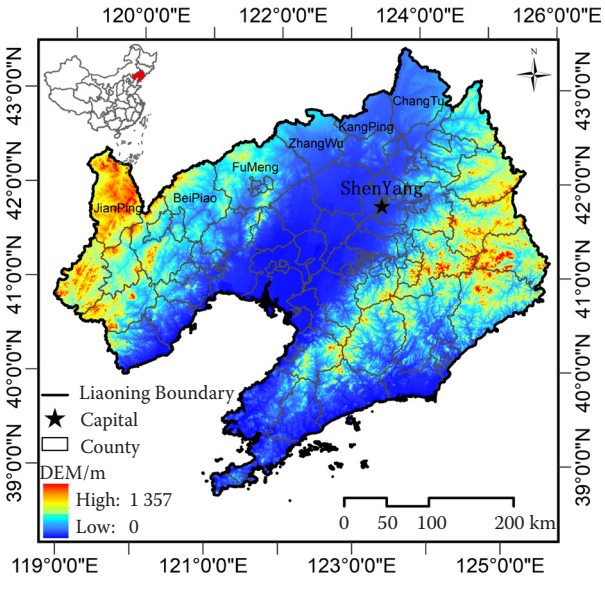

Figure 1. Study area

https://doi.org/10.17221/106/2021-SWR

from 1961 to 2015; four stations in Hebei Province from 1961 to 2015; and four stations in the Inner Mongolia Autonomous Region from 1961 to 2015. The soil data were based on a 1 : 1 000 000 digital soil map jointly released by the Nanjing Institute of Soil Science, the Chinese Academy of Sciences, and the Soil Environment Division of the Ministry of Agriculture of China. The vector data in ARC/INFO (Ver. 7.1) software and the converted E00 file data were used in the COVERAGE format. Soil particle composition queries were performed using Chinese Soil Types (Volume 2), Liaoning Soil Types, and Liaoning Soil as references. Additional data consisted of vector data from the administrative divisions of Liaoning, sediment runoff data collected by 20 water conservation observation fields (2013–2015), and soil conservation management survey data.

Hillslope-erosion assessment. Hillslope-erosion was assessed using the empirical USLE model. The factors comprehensively incorporated into the USLE model are easily accessible and practical parameters, making the model the most mature method for estimating the soil erosion thus far. It can be written as:

$$A = R \times K \times LS \times C \times P \quad (1)$$

where:

A – average annual soil loss rate (t/ha^{-1}·a^{-1});
R – rainfall erosivity factor (MJ·mm·ha^{-1}·h^{-1}·a^{-1});
K – soil erodibility factor (t·h·MJ^{-1}·mm^{-1});
LS – topographic factor;
C – vegetation coverage and management factor;
P – conservation supporting practice factor.

In the present study, the average annual soil loss was estimated on a 10 × 10 m cell basis resolution by overlaying the five digital parameter layers (R, K, LS, C, P) in vector format. Here, each cell is assumed as a closed plot where surface flow cannot enter a cell from another cell. A similar assumption was made by Fistikoglu and Harmancioglu (2002).

The semi-monthly rainfall erosivity for each year was calculated by applying the rainfall erosivity model of Zhang et al. (2002) to the 55-year (1961–2015) daily rainfall observation data collected from 39 stations in four provinces (Liaoning, Jilin, Hebei, and Inner Mongolia). These results were used to calculate the annual and average annual rainfall erosivity for each station over 55 years. Kriging of the average annual rainfall erosivity of each weather station was used to generate spatial data for the rainfall erosivity factor (R) in Liaoning. The model of Shirazi and Boersma (1984) and corrected results of Zhang et al. (2007) were used to calculate the soil erodibility K for each soil type in Liaoning. The results were input into a soil type vector map to obtain the soil erodibility factor (K) for Liaoning. The topographic factor (LS) was calculated based on the 1 : 50 000 DEM using the watershed LS software (LS-Reg) developed by Yang et al. (2010) and Zhang et al. (2012), by setting the threshold to 100 000 m^2 and the cut-off to 0.5 (slope gradient < 2.75°) or 0.7 (slope gradient ≥ 2.75°). During the development of the LS-Reg software, a dirty area of 6 km as a buffer area was set (Note: 6 km in China's Northeast; 3 km in China's loess area) to ensure the slope length can be calculated with the watershed as the boundary instead of other boundaries (such as an administrative district, rectangle, etc.). A threshold of 100 000 m^2 was set to ensure that the watershed extracted in this study can better correspond to the results of the First Water Conservancy Survey in Liaoning Province.

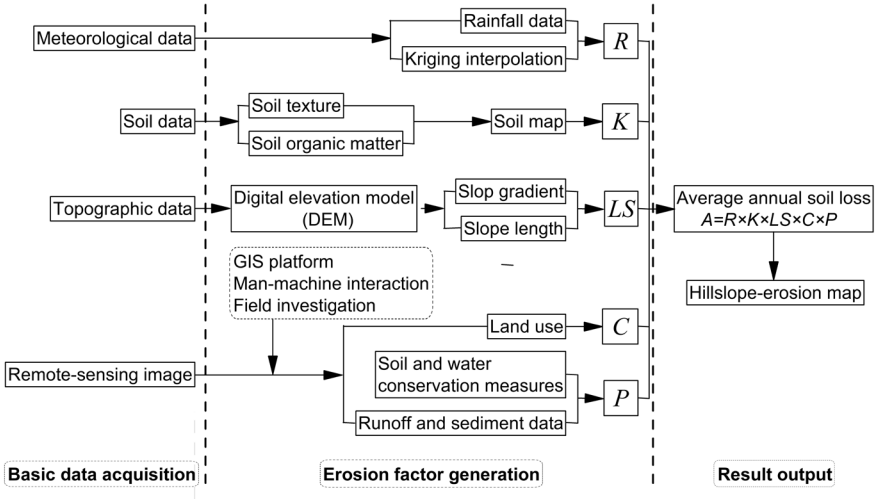

Figure 2. Flowchart for the hillslope-erosion estimation
R – rainfall erosivity factor; K – soil erodibility factor; LS – topographic factor; C – egetation coverage and management factor; P – conservation supporting practice factor

https://doi.org/10.17221/106/2021-SWR

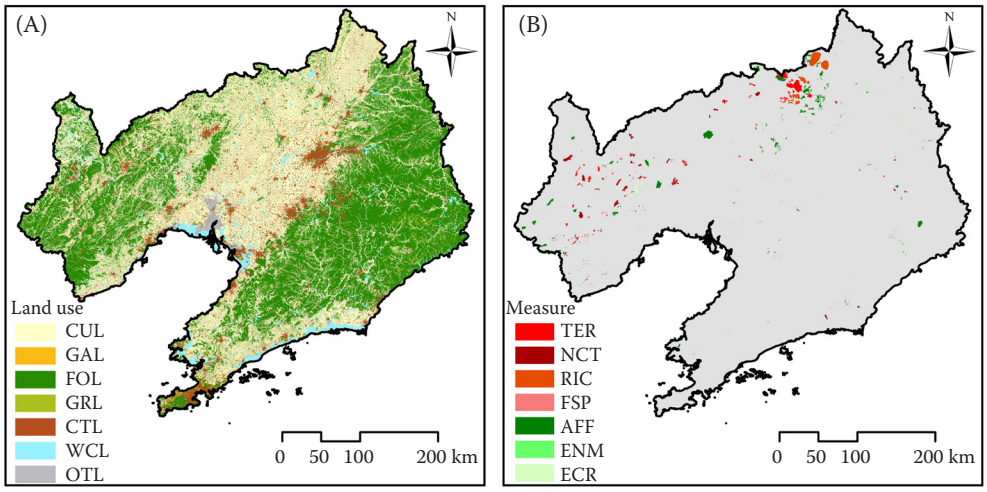

Figure 3. Land use (A) and soil and water conservation measure (B)
CUL – cultivated land; GAL – garden land; FOL – forestland; GRL – grassland; CTL – construction and traffic land; WCL – water conservancy land; OTL – other land; TER – terraces; NCT – no-tillering cultivation tillage; RIC – ridge change; FSP – fish-scale pit; AFF – afforestation; ENM – enclosure management; ECR – ecological restoration

The land use was first interpreted by combining the RS image data and the field survey information (Figure 3A). The human-computer interaction interpretation method is one of the most basic RS image information extraction methods (Yang et al. 2020). Moreover, the attribute value (Table 1) was assigned to each land use patch in ArcGIS (Ver. 10.2) to obtain the vegetation coverage and management factor (C). The C factor value is estimated according to the relationship between the management factor (C) and vegetation coverage (c) proposed in the soil erosion study by Cai et al. (2000). The expression is:

$$\begin{cases} C = 1 & c = 0 \\ C = 0.6508 - 0.3436 \log c & 0 \le c < 78.3\% \\ C = 0 & c \ge 78.3\% \end{cases} \quad (2)$$

Where, the minimum value of C should be 0, that is, no soil loss occurs, and c is 78.3%; and the maximum value of C is 1, which is the standard condition, and the calculated value of c is about 0.1%, which is the result of the mathematical calculation, C can be regarded as 0 in practical applications. When $c > 78.3\%$, C can be regarded as 0.

This method has a higher calculation accuracy and does not require on-site sampling in the field, which is the development direction of calculating the C value in the future. However, due to the discontinuity of the image time series and geographical limitations, the calculation results of the C value were relatively higher so that the method was not used in this experiment. The C value (Table 1) of this study was determined in accordance with China's soil erosion dynamic monitoring technical guidelines and the research results of Zhang et al. (1992, 2006), Cai et al. (2000), and Song et al. (2009).

The water conservation survey data and the RS data were used to plot a soil and water conservation

Table 1. Vegetation coverage and management factor (C) for the different land use classes

Land use secondary class	C factor
Dry land	0.24
Paddy field	0.18
Irrigated land	0.1
Forestland	0.0025
Shrubland	0.006
Other forestland	0.184
Artificial pastures	0.0032
Natural pastures and grassland	0.01
Other grassland	0.455
Rural settlement	0.03
Urban settlement	0.153
Commercial and public uses	0.153
Mining and manufacturing sites	0.01
Transportation and highway	0.22
Water conservancy land	0
Other land	0.5

https://doi.org/10.17221/106/2021-SWR

measure distribution map (Figure 3B). The *P* factor refers to the ratio of the soil loss after implementation of the water and soil conservation measures, such as contour farming, contour strip planting, or repairing ridges, terraces, etc., to the soil loss on the standard plot when the other conditions are the same. Due to the inconsistent slopes of the plots, the amount of soil loss in all the plots should be corrected to the amount of soil loss on the slope of 5° in the calculation (Fan et al. 2011). The correction formula is:

$$A_{i5} = S_5 \frac{A_i}{S_i} \quad (3)$$

where:

A_{i5} – the amount of soil loss on the i^{th} plot corrected to a 5° slope (t/km^2);

A_i – the amount of soil loss on the i^{th} plot (t/km^2);

S_5 – the slope factor of the 5° slope;

S_i – the slope factor on the i^{th} plot.

The slope factor is calculated according to the method proposed by Renard et al. (1997) and Liu et al. (1994). The formula is:

$$\begin{cases} S = 10.8 \sin\theta + 0.03 & \theta < 5° \\ S = 16.8 \sin\theta - 0.50 & 5 \le \theta < 10° \\ S = 21.9 \sin\theta - 0.96 & \theta \ge 10° \end{cases} \quad (4)$$

Table 2. Conservation supporting practice factor (*P*) for the different measure classes

Measure class	*P* factor	Original source
Terraces	0.029	Zhang et al. (1992)
No-tillering cultivation tillage	0.121	Zhang et al. (1992)
Ridge change	0.248	calculation
Fish scale pit	0.123	calculation
Afforestation	0.497	Chen et al. (2011)
Enclosure management	0.497	Chen et al. (2011)
Ecological restoration	0.464	calculation

where:

S – the slope factor;

θ – the slope gradient.

In addition, the results of the *P* value by Zhang et al. (1992) and Chen et al. (2011) were also used to assign an attribute value for the soil and water conservation measure (Table 2). Finally, the vector data of each factor were rasterised, and the product of the factors was calculated using ArcGIS (Ver. 10.2) to generate the average annual soil loss rate (*A*). The hillslope-erosion intensity assessment process is shown in Figure 2, and the results are shown in Figure 4 and Figure 6A.

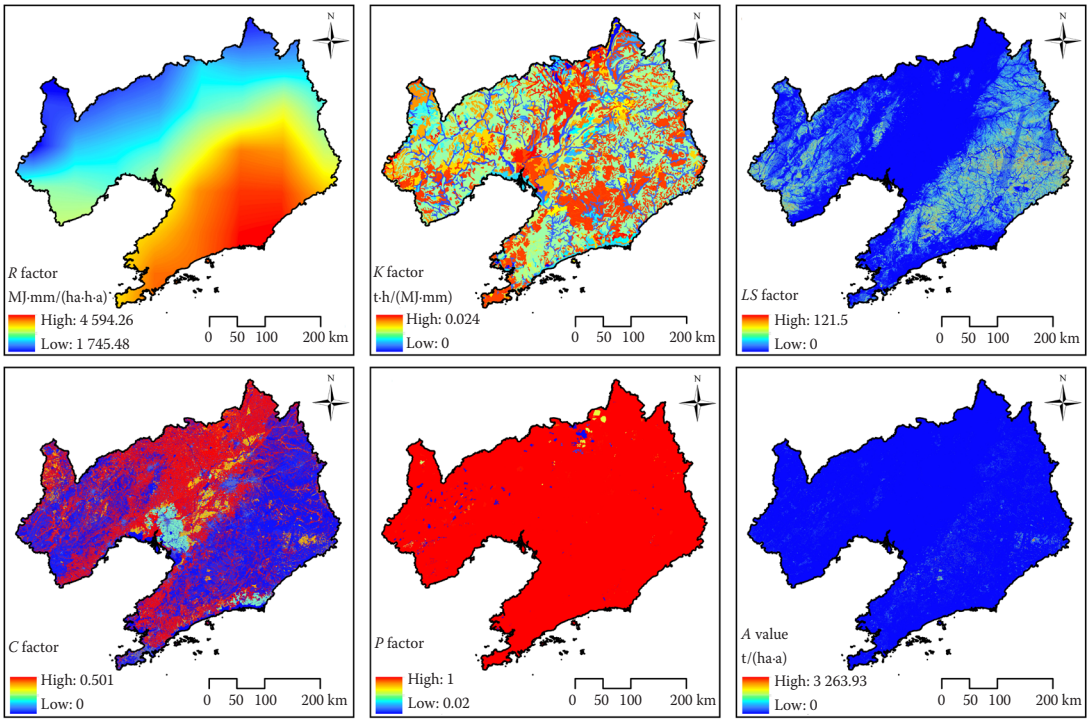

Figure 4. Rainfall erosivity factor (*R*), soil erodibility factor (*K*), topographic factor (*LS*), vegetation coverage and management factor (*C*), conservation supporting practice factor (*P*), and average annual soil loss rate (*A*)

https://doi.org/10.17221/106/2021-SWR

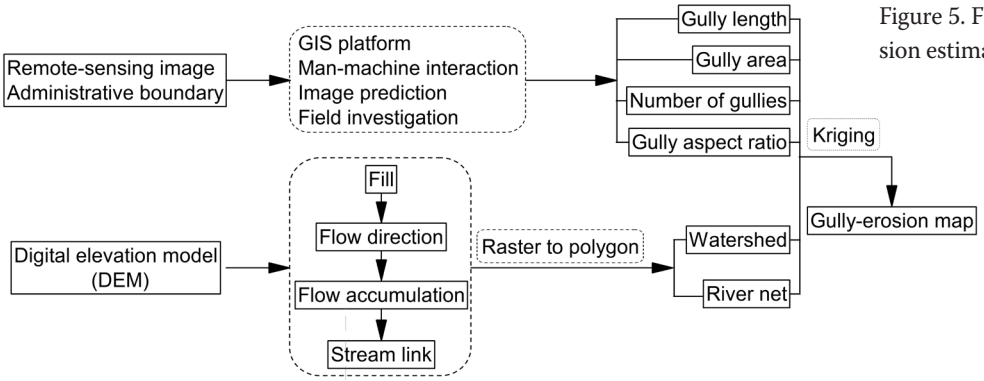

Figure 5. Flowchart for the gully-erosion estimation

Gully-erosion assessment. The gully-erosion intensity was estimated using the gully density. The gullies in Liaoning were interpreted using the human-computer interaction with ArcGIS (Ver. 10.2). For the RS images, a line was drawn along each gully bed from the origin to the opening and used as the scale in delineating the gully edge. All the gullies were coded to facilitate the establishment of a spatial database, and the data quality was guaranteed by interpretating the images with an accuracy higher than 90%. In order to have no omissions or misidentification occurring for the spatial data, 5% of the total number of gullies in this study was extracted to validate them by field survey and cross-verification.

The intensity of the gully-erosion was assessed by taking a watershed less than 50 km^2 as a unit to accurately identify the level of the gully-erosion in the study area. Some natural properties, i.e., climate, vegetation, land use types, are similar or consistent within the same small watershed. Each density of the watershed was input to the gully GIS spatial database and manipulated by Kriging in ArcGIS (Ver. 10.2) to generate a spatial distribution map for the gully density. The assessment process for the gully-erosion intensity is shown in Figure 5, and the results are shown in Figure 6B.

Data extraction. This study of hillslope-erosion used the Technical standard for comprehensive control of soil erosion in the black soil region of China (SL 446-2009) and the Technical standards for comprehensive treatment of water and soil erosion in the earth rock mountain areas of northern China (SL 665-2014) issued by the Ministry of Water Resources (Table 3). The hillslope-erosion was classified into six levels (micro, slight, moderate, high, very high, and severe). Adopting the gully-erosion grading criteria of the Ministry of Water Resources (< 1 km/km^2: slight gully-erosion) would have led to the conclusion that there was no gully-erosion in Northeast China. However, there is severe gully-erosion in Northeast China. The particularities of the gully-erosion were considered in Northeast China to identify six levels of gully-erosion based on the gully density (Yan et al. 2006), i.e., micro (0–0.1 km/km^2), slight (0.1–0.25 km/km^2), moderate (0.25–0.5 km/km^2), high (0.5–0.75 km/km^2), very high (0.75–1.0 km/km^2), and severe (>1.0 km/km^2).

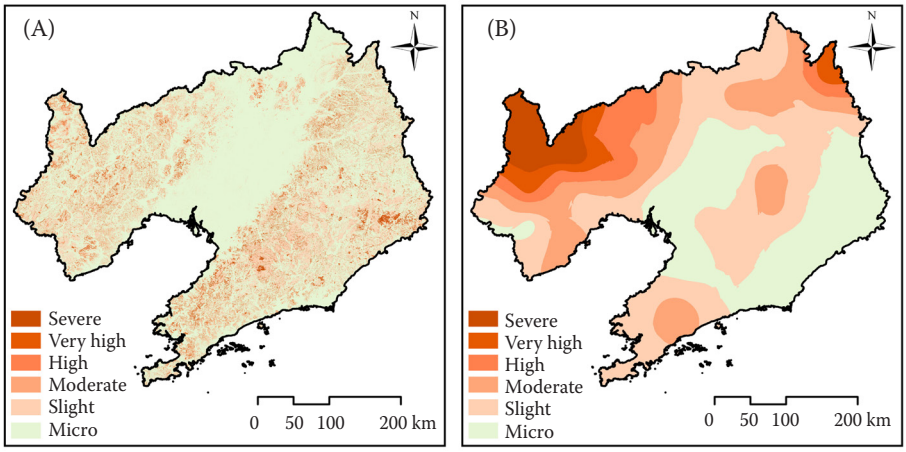

Figure 6. Spatial distribution of the hillslope-erosion (A) and gully-erosion (B)

https://doi.org/10.17221/106/2021-SWR

Table 3. Technical standard for the class and grade of soil erosion

Class	Amount of soil erosion (t/km²·a)	
	SL 446-2009	SL 665-2014
Micro	≤ 200	≤ 200
Slight	200–1 200	200–1 000
Moderate	1 200–2 400	1 000–2 500
High	2 400–3 600	2 500–4 000
Very high	3 600–4 800	4 000–6 000
Severe	> 4 800	> 6 000

Adopting ArcGIS (Ver. 10.2), the land use was overlaid on spatial distribution maps for the hillslope-erosion amount and the gully density. The slope and reclassify functions were used to extract and divide the slope gradient into 25 levels at 1° intervals. The effect of the slope gradients above 25°, corresponding mostly to forestland, on the soil erosion will be explored in a future study and is not discussed here. The aspect and reclassify functions were used to extract and classify the slope aspect into 16 levels in 22.5° intervals (Table 5). The curvature and reclassify functions were used to extract and classify the slope shape into three categories, i.e., concave (curvature < 0), straight (curvature = 0), and convex (curvature > 0). The distribution of the hillslope- and gully-erosion from the perspectives of erosion intensity and land use, as well as the slope gradient, aspect, and shape were obtained by data processing.

RESULTS AND DISCUSSION

Relationship of hillslope- and gully-erosion under different erosion intensities. Significant regional variation can be observed in the spatial distributions of the hillslope- and gully-erosion (Figure 6). The hillslope-erosion intensity exhibited a saddle-shaped distribution that inclined from the east and the west to the middle, i.e., the hillslope-erosion was severe on the east and west sides (the low hills in Eastern and Western Liaoning), but low in the middle (the plains in the lower reach of the Liaohe River) (Figure 6A). The spatial distribution of the hillslope-erosion followed the same pattern as the terrain of the study area, indicating the dominant role played by the topographic factors (the slope gradient, aspect, and shape, etc.) among the factors affecting the hillslope-erosion (precipitation, terrain, vegetation, soil, etc.). The gully-erosion intensity exhibited a stepwise increasing trend from the southeast to northwest (Figure 6B) that depended mainly on the vegetation coverage and human factors.

The attribute query function of ArcGIS (Ver. 10.2) was used to obtain the area distributions of the two types of soil erosion under different erosion intensities (Table 4). The effect of the erosion intensity on the distributions of the hillslope- and gully-erosion was then analysed. The hillslope-erosion in the study area was dominated by micro erosions, which accounted for 75.29% of the total erosion area. Slight erosions accounted for 13.51% of the total erosion area, compared to a contribution of less than 12% from erosions at or above the moderate level. The gully-erosion was dominated by micro, slight, and moderate erosions, accounting for 29.32%, 35.41%, and 18.70%, respectively, of the total erosion area, compared to a contribution of less than 17% from erosions at and above the high level. The development of the gully-erosion was more severe compared to the hillslope-erosion. This distribution results from the main topography of Liaoning being constituted from the central plains, which are dominated by siltation and are the main micro erosion area. In comparison, the high vegetation coverage and small watershed area make the high altitudes and steep slopes in the east less prone to erosion than the topography would suggest. Most of the area between these two regions comprises vast stretches of slope farmlands, with mainly slight and moderate erosion. The significant effect of human activities has turned this land into a main soil erosion area. The distribution ratios of various gully-erosion levels indicate mostly low-level gully-erosion. However, there is a large proportion of slight and moderate erosion with the potential to develop into high-level gully-erosion. As a result, the hillslope-erosion tends to be aggravated by this strong potential to

Table 4. Area corresponding to the different classes of hillslope- and gully-erosion

Class	Hillslope-erosion		Gully-erosion	
	(km²)	(%)	(km²)	(%)
Micro	111 525.47	75.29	43 437.64	29.32
Slight	20 016.12	13.51	52 452.24	35.41
Moderate	6 608.61	4.46	27 708.12	18.70
High	3 226.06	2.18	10 783.62	7.28
Very high	1 941.84	1.31	5 950.89	4.02
Severe	4 814.43	3.25	7 800.02	5.27

https://doi.org/10.17221/106/2021-SWR

a certain extent. Thus, prompt effective prevention and control measures are required to prevent accelerated progression to high-level hillslope-erosion.

Relationship of hillslope- and gully-erosion under different land uses. Land use determines the distribution of the vegetation and the pattern of human activities, and thus affects the form, speed, and intensity of the soil erosion. To examine the effect of land use on the distributions of the hillslope- and gully-erosion, the land use was overlaid on spatial distribution maps for the hillslope-erosion amount and gully density to obtain the distributions of the hillslope-erosion amount and gully density under different land uses (Figure 7).

Figure 8 indicated that the hillslope-erosion amount and gully density were highest on the cultivated land, followed by forestland. The slope erosion amount and gully density of cultivated land are 625.01 t/km^2·a and 0.06 km/km^2 larger than that of the forestland, respectively. The low hills that constitute a large proportion of the study area, along with the central plains, contain much cultivated land with low vegetation coverage and the highest level of human activities in the region, leading to the most intensive soil erosion, which was consistent with the results of Li et al. (2019) and Jia et al. (2019). Forestlands have high vegetation coverage, but are mostly found in areas with steep slopes. As the slope gradient plays a key role in the soil erosion, the forestland has a high soil erosion intensity. Grasslands have high vegetation coverage and low slopes and, therefore, a lower soil erosion intensity than the forestland. Very little hillslope-erosion, but severe gully-erosion occurs in lands used for construction and traffic, and in the water conservancy lands, mainly because of human factors and concentrated run-off.

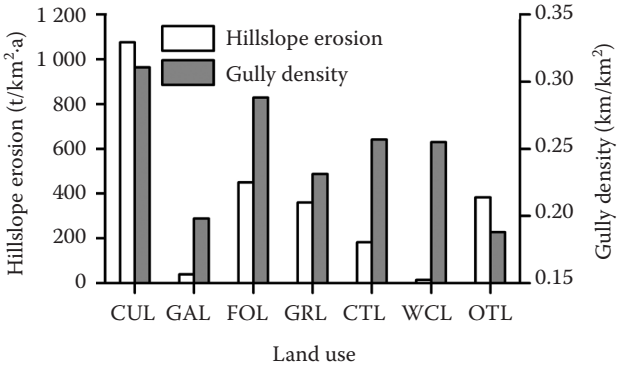

Figure 7. Effect of land use on the hillslope-erosion amount and gully density

CUL – cultivated land; GAL – garden land; FOL – forestland; GRL – grassland; CTL – construction and traffic land; WCL – water conservancy land; OTL – other land

Relationship of hillslope- and gully-erosion under different slope gradients. The slope gradient is a major topographic factor that determines the volume and velocity of the surface run-off and, thus, directly affects the intensity with which the run-off scours a surface. The raster data for the slope gradient was converted into vector data, which was overlaid on spatial distribution maps for the hillslope-erosion amount and gully density to analyse the effect of the slope gradient (Figure 8).

Figure 8 shows that the effect of slope gradient on the distributions of hillslope- and gully-erosion differed observably in the study area. As the slope gradient increased, the hillslope-erosion first increased from 7.23 to 1 393.28 t/km^2·a and then decreased steadily to 1 232.11 t/km^2·a. The amount of hillslope-erosion reaches a maximum of 1 393.28 t/km^2·a at a 14° slope gradient. However, the hillslope-erosion levelled off at slope gradients of 9–14°. The hillslope-erosion amount had an approximate power law function in the slope gradient ($y = -6.0078x^2 + 201.34x - 209.58$, $R^2 = 0.9441$), which was consistent with the findings of Zhang et al. (1992) and Pan et al. (2012). The gully density varied markedly with the slope gradient: the gully-erosion increased from 0.20 to 0.41 km/km^2 and then decreased sharply to 0.23 km/km^2 as the slope gradient increased. The gully density peaked at 0.41 km/km^2 at a 6° slope gradient. The fitting equation for the gully density versus the slope gradient ($y = -0.0006x^2 + 0.0113x + 0.3058$, $R^2 = 0.5801$) showed a less significant correlation than that of the hillslope-erosion with the slope gradient. However, the gully density

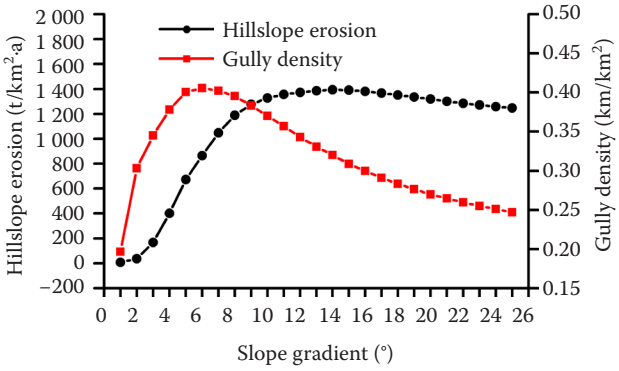

Figure 8. Effect of the slope gradient on the hillslope-erosion amount and gully density

https://doi.org/10.17221/106/2021-SWR

increased exponentially for slope gradients below 6° ($y = -0.2114x^{0.4027}$, $R^2 = 0.9480$), which was consistent with the results of Wang and Fan (2019).

Threshold slope gradients of 14° and 6°, respectively, were identified for the hillslope- and gully-erosion in the study area from the analyses above, where the slope gradient affected the hillslope-erosion more obviously than the gully-erosion. Below the threshold slope gradient, the amount of hillslope-erosion and the gully density both increased with the slope gradient. That is, the slope gradient is the primary factor affecting the development of hillslope- and gully-erosion over this regime, because the shearing force from the run-off on the soil particles increases with the slope gradient (Guan et al. 2019), making the soil less stable. Thus, gravitational erosion plays an important role in the hillslope- and gully-erosion. The increase in the soil erosion from the gravitational erosion in turn increases the intensities of the hillslope- and gully-erosion. There was a significant difference in the effect of the slope gradient on the hillslope-erosion and gully density above the threshold slope gradient. For slope gradients above 6°, the gully density decreased markedly as the slope gradient increased (Ranzi et al. 2012), indicating that the slope gradient was no longer the primary factor affecting the development of the gully-erosion. Other factors, such as the slope length and shape, the water catchment area, and topographical fluctuations, exert a larger impact than the slope gradient in this regime (Yan et al. 2007). The study area terrain with slope gradients above 6° is dominated by a vast area of low hills with a low average slope length and a small catchment area. Thus, rainfall rapidly runs off this terrain, and the reduced infiltration cannot generate concentrated surface runoff, thereby decreasing the run-off shear force. Moreover, the proportion of forestland increases with the slope gradient, effectively intercepting the rainwater and alleviating the impact of raindrops on the ground. This activity couples with the interception and storage of rainwater by litter on the ground to inhibit the development of gully-erosion.

Relationship of hillslope- and gully-erosion under different slope aspects. The slope aspect determines the direction of the surface run-off; affects the secondary distribution of the water, nutrient, light, heat, and the selective growth of plants; and indirectly affects the erosion intensity of the run-off on a surface (Mi et al. 2021; Zhang et al. 2021; Wang et al. 2021; Chen et al. 2022). The raster data for the slope aspect was converted into vector data, which was overlaid on the spatial distribution maps for the hillslope-erosion amount and gully density to determine the effect of the slope aspect (Figure 9).

Figure 9 indicates that the slope aspect markedly affected the distributions of the hillslope- and gully-erosion. A highly asymmetric soil erosion pattern and intensity were observed under the different slope aspects because of the differences in the soil moisture, rainwater erosivity, the wind direction at the time of the rainfall, and vegetation growth environments (Chen et al. 2006). The amount of hillslope-erosion under the different slope aspects was in the range of 5 74.21–795.17 t/km^2·a. There was an observably more hillslope-erosion amount on sunny slopes (778.68 t/km^2·a) than shady slopes (629.22 t/km^2·a). The amount of hillslope-erosion distribution was heart-shaped around an axis of the SSE aspect and reached a maximum on the SSE aspects (Figure 9A). This distribution is explained as follows: (1) Sunny slopes receive more sunshine than shady slopes. This high radiation intensity, coupled with the northeast location of the study area, which is characterised by significant intra-year temperature changes and distinct freeze-thaw cycles, can deteriorate the structural stability of the surface soil and decrease the erosion resistance (Yan et al. 2005). (2) In the spring snow-melting season, the surface soil on the sunny slopes thaws rapidly, whereas the slow thawing of the thick frozen soil layer under the surface soil prevents the surface run-off from infiltrating

Table 5. Slope aspect classification

Slope aspect	Azimuth angle (°)
North (N)	0–22.5
North-northeast (NNE)	22.5–45
Northeast (NE)	45–67.5
East-northeast (ENE)	67.5–90
East (E)	90–112.5
East-southeast (ESE)	112.5–135
Southeast (SE)	135–157.5
South-southeast (SSE)	157.5–180
South (S)	180–202.5
South–southwest (SSW)	202.5–225
Southwest (SW)	225–247.5
West–southwest (WSW)	247.5–270
West (W)	270–292.5
West–northwest (WNW)	292.5–315
Northwest (NW)	315–337.5
North–northwest (NNW)	337.5–360

https://doi.org/10.17221/106/2021-SWR

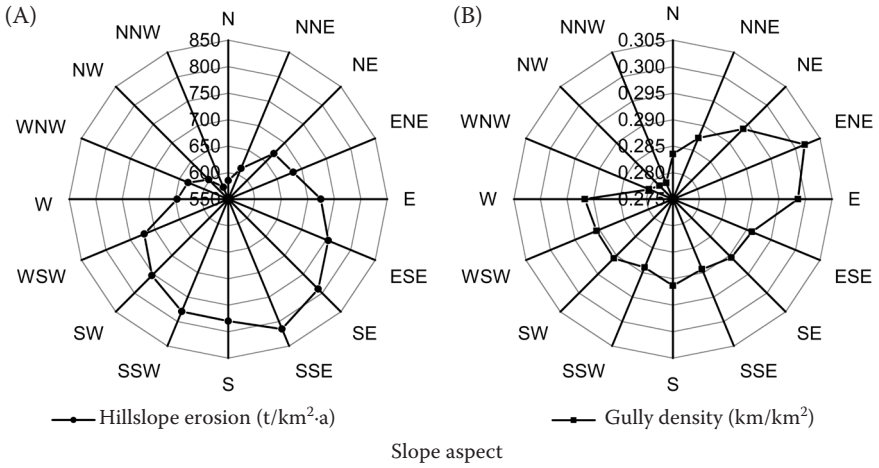

Figure 9. Effect of the slope aspect on the hillslope-erosion amount (A) and gully density (B)
For the slope aspect abbreviations see the Table 5

the soil. Therefore, intense runoff is generated rapidly, and the strong run-off shear force (Liu & Jing 1999) produces high erosion. (3) In the summer, the southeast monsoon climate of the study area results in concentrated rainfall from June to August, which accounts for 60–70% of the total annual rainfall. The sunny slopes are also windward slopes, where the large angle between the raindrops and the slope surface produces a strong splashing impact on the slope surface and causes higher erosion on the sunny slopes than on the shady slopes (Yan et al. 2005).

The gully densities of slopes with different aspects were in the range of 0.28–0.31 km/km^2, with an average of 0.29 km/km^2. The slope aspect affected the gully density less significantly than the amount of hillslope-erosion, which is attributed to the unique characteristics of the gully-erosion in the region caused by the vast area of low hills. Once a gully is formed, the absence of a clear orientation in the development of a gully (erodes from the original gully head, expands to the edge, cuts down to the gully bed, and generates a branch gully, etc.) decreases the effect of the slope aspect on the gully-erosion (Wang et al. 2012), which is signally different from observations of gullies with different slope aspects in the Loess Plateau (Chen et al. 2006). The above analyses show that the slope aspect was not the primary factor affecting the gully-erosion in Northeast China. However, the slope aspect slightly affected the intensity of the gully-erosion. The highest gully density was observed on slopes with dominant E, ENE, and NE aspects. The lowest gully density was observed on slopes with dominant WNW, NW, and NNW aspects. The gully density on the ENE-facing slopes was substantially higher than on the slopes with other directional aspects (Figure 9B). Therefore, the influence of the slope aspect on the gully-erosion cannot be neglected. The slope aspect impacts the gully density distribution in the following ways: (1) The study area has a saddle-shaped topography, tilting toward the centre from the east and west, which leads to higher average gradients for the E, ENE, and NE aspects. (2) In winter, the northeast monsoon climate produces heavier rain and snow on the E-, ENE-, and NE-facing slopes than on the slopes with other directional aspects. Thus, in the spring, the run-off caused by the snow thawing on these aspects is more abundant and concentrated than on the slopes with the other aspects, increasing the run-off shear force and ultimately the gully-erosion intensity. Therefore, the contribution of the slope aspect to the gully-erosion intensity should not be denied.

Relationship of hillslope- and gully-erosion under different slope shapes. The slope shape determines both the catchment area, and the run-off distribution and velocity and is, therefore, an important factor affecting the soil erosion. Few studies have been performed on the effect of the slope shape on the soil erosion in China or abroad and are even more rare on Northeast China. The raster data for the slope shape were converted into vector data and overlaid onto the spatial distribution maps of the hillslope-erosion amount and the gully density to analyse the effect of the slope shape (Figure 10).

Figure 10 shows that the amount of hillslope-erosion on the concave, convex, and straight slopes was

https://doi.org/10.17221/106/2021-SWR

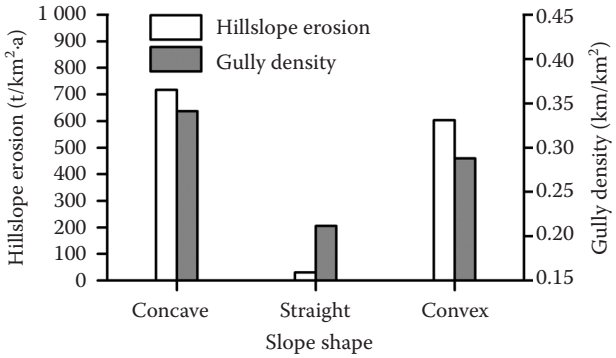

Figure 10. Effect of the slope shape on the hillslope-erosion amount and gully density

716.62, 603.98, and 30.24 t/km^2·a, respectively, and the corresponding gully density was 0.32, 0.29, and 0.21 km/km^2. The highest hillslope-erosion amount and gully density was observed for concave slopes, followed by convex and straight slopes (Yu & Wei 2010). Straight slopes had a negligible impact on the hillslope-erosion, but had a high impact on the gully-erosion. A concave slope has a rather large catchment area. The upper portion of the area has a straight slope or convex slope, with ridges on both sides. The run-off generated at the top of the catchment area accumulates rapidly on the concave slope and eventually reaches the gully bed as concentrated run-off. The strong run-off shear force continuously increases the surface scouring and cuts off the gully bed, generating a high soil erosion intensity. Straight slopes have a relatively flat surface with small catchment areas, inhibiting run-off concentration and intensification. Thus, the run-off shear force is weak and less able to cause hillslope-erosion. Straight slopes generally represent a transition zone between concave and convex slopes, for which the slope gradient and length affect the gully-erosion more than slope shape.

CONCUSIONS

On the basis of a coupling analysis of hillslope- and gully-erosion, the important patterns and rules between the two types of soil erosion were identified. Hillslope-erosion tends to be aggravated by the development of gully-erosion. Prompt effective prevention measures are required to prevent the certain acceleration to high-intensity hillslope-erosion. Cultivated land has the highest level of anthropogenic activities and the most intense hillslope- and gully-erosion, which was a key area for the prevention and control of soil erosion. The terrain (slope gradient, slope aspect, and slope shape) was the crucial factor affecting hillslope- and gully-erosion. The slope gradient and aspect affect hillslope-erosion more obviously than gully-erosion. The concave- and convex-slope have a marked influence on the hillslope- and gully-erosion. A straight-slope has a negligible impact on the hillslope-erosion, but has a relatively higher impact on the gully-erosion. The findings on the hillslope- and gully-erosion and their coupling mechanism will improve our understanding of soil erosion across a slope-gully system in China's Northeast Region, and contribute to increasing controlling efforts to prevent soil erosion.

Acknowledgement: We are grateful to the Liaoning Provincial Water Resources Department and Soil and Water Conservation Bureau of the People's Republic of China for providing most of the basic datasets. We also sincerely thank the reviewers and editors for their valuable and constructive comments.

REFERENCES

Achten W.M.J., Dondeyne S., Mugogo S., Kafiriti E., Poesen J., Deckers J., Muys B. (2008): Gully erosion in South Eastern Tanzania: Spatial distribution and topographic thresholds. Zeitschrift für Geomorphologie, 52: 225–235.

Aderemi A., Iyamu F. (2012): Risk assessment analysis of accelerated gully erosion in Ikpoba Okha local government area of Edo State, Nigeria. Environment and Natural Resources Research, 3: 68–76.

Al-Abadi A.M., Al-Ali A.K. (2018): Susceptibility mapping of gully erosion using GIS-based statistical bivariate models: A case study from Ali Al-Gharbi District, Maysan Governorate, southern Iraq. Environmental Earth Sciences, 77: 249–269.

Alireza A., Biswajeet P., Khalil R., Mojtaba Y., Reza P.H., Luigi L. (2018): Spatial modelling of gully erosion using evidential belief function, logistic regression, and a new ensemble of evidential belief function-logistic regression algorithm. Land Degradation & Development, 29: 4035–4049.

Anderson J.R., Thampapillai J. (1990): Soil conservation in developing countries. Social and Economic Studies, 39: 201–204.

Anees M.T., Abdullah K., Nawawi M.N.M., Norulaini N.A.N., Syakir M.I., Omar A.K.M. (2018): Soil erosion analysis by RUSLE and sediment yield models using remote sensing and GIS in Kelantan state, Peninsular Malaysia. Soil Research, 56: 356–372.

https://doi.org/10.17221/106/2021-SWR

Avijit M. (2018): Soil erosion estimation using RUSLE and GIS techniques – A study of a plateau fringe region of tropical environment. Arabian Journal of Geosciences, 11: 335–353.

Bartsch K.P., Miegroet H., Boettinger J., Dobrowolski J.P. (2002): Using empirical erosion models and GIS to determine erosion risk at Camp Williams. Journal of Soil & Water Conservation, 57: 29–37.

Boggs G., Devonport C., Evans K., Puig P. (2001): GIS-based rapid assessment of erosion risk in a small catchment in the wet/dry tropics of Australia. Land Degradation & Development, 12: 417–434.

Cai C.F., Ding S.W., Shi Z.H., Huang L., Zhang G.Y. (2000): Study of applying USLE and geographical information system IDRISI to predict soil erosion in small watershed. Journal of Soil and Water Conservation, 14: 19–24. (in Chinese)

Chen H., Fang H.Y., Cai Q.G., Lei T.W., Liang G.L. (2006): Comparison of different aspect of erosion evolvement in the Loess Hilly Area: A case study of Wangjiagou catchment of Western Shanxi Province. Resources Science, 28: 176–184. (in Chinese)

Chen J., Zhang X.J., Li Q.Y., Tao J.P. (2022): Relationships between competition intensity and leaf phenotypic plasticity of woody plants in subalpine forests on different slope directions. Acta Ecologica Sinica, 42: 1–10. (in Chinese)

Chen Z.F., Shi D.M., Guo H.Z., Jiang G.Y., Tang X.W. (2011): Study on response of slope erosion characteristics in Purple Hilly Region. Journal of Soil and Water Conservation, 25: 52–57. (in Chinese)

Conoscenti C., Angileri S., Cappadonia C., Rotigliano E., Agnesi V., Maerker M. (2014): Gully erosion susceptibility assessment by means of GIS-based logistic regression: A case of Sicily (Italy). Geomorphology, 204: 4035–4049.

Costa F.M., Bacellar L.D.A.P. (2007): Analysis of the influence of gully erosion in the flow pattern of catchment streams, Southeastern Brazil. Catena, 69: 230–238.

Daba S., Rieger W., Strauss P. (2003): Assessment of gully erosion in eastern Ethiopia using photogra-mmetric techniques. Catena, 50: 273–291.

Dabral P.P., Baithuri N., Pandey A. (2008): Soil Erosion Assessment in a Hilly Catchment of North Eastern India Using USLE, GIS and Remote Sensing. Water Resources Management, 22: 1783–1798.

Fan J.R., Wang N.Z., Chen G., Jiao J., Xie Y. (2011): Practice factor of soil and water conservation in Northeastern China. Science of Soil and Water Conservation, 9: 75–78. (in Chinese)

Fistikoglu O., Harmancioglu N.B. (2002): Integration of GIS with USLE in assessment of soil erosion. Water Resoures Management, 16: 447–467.

Ganasri B.P., Ramesh H. (2016): Assessment of soil erosion by RUSLE model using remote sensing and GIS – A case study of Nethravathi Basin. Geoscience Frontiers, 7: 953–961.

Grepperud S. (1995): Soil conservation and governmental policies in tropical areas: Does aid worsen the incentives for arresting erosion. Agricultural Economics, 12: 129–140.

Guan C., Zhang S.W., Wang R.H., Yang J.C., Yue S.P., Yu L.X., Wang W. (2019): Coupling analysis between ridge direction and gully erosion of sloping cultivated lands in the Sancha River watershed. Resources Science, 41: 394–404. (in Chinese)

Hu G., Wu Y.Q., Liu B.Y., Yu Z.T., You Z.M., Zhang Y.G. (2007): Short-term gully retreat rates over rolling-hill areas in Black Soil of Northeast China. Catena, 71: 321–329.

Jha V.C., Kapat S. (2009): Rill and gully erosion risk of lateritic terrain in South-Western Birbhum District, West Bengal, India. Revista Sociedade & Natureza, 21: 141–158.

Jia Y.F., Wu M., Liu M.B. (2019): Soil erosion characteristics of different land use types in thawing period in hilly areas of Northeast China. Journal of Shenyang Agricultural University, 50: 747–752. (in Chinese)

Karamage F., Zhang C., Kayiranga A., Shao H., Fang X., Ndayisaba F., Nahayo L., Mupenzi C., Tian G.J. (2016): USLE-based assessment of soil erosion by water in the Nyabarongo river catchment, Rwanda. Environment Research and Public Health, 13: 835–851.

Li M. J., Li T. Q., Zhu L. Q., Zhang S.W., Zhu W.B., Zhang J.J. (2019): Effect of land use change on gully erosion in black soil region of Northeast China in the past 50 years: A case study in Kedong county. Geographical Research, 38: 2913–2926. (in Chinese)

Liu B.Y. (2003): Discussion on problems about soil degradation and sustainable utilization in typical black soil region. Soil and Water Conservation in China, 12: 28–29. (in Chinese)

Liu B.Y., Nearing M.A., Risse L.M. (1994): Slope gradient effects on soil loss for steep slopes. Transactions of the ASAE, 37: 1835–1840. (in Chinese)

Liu X.J., Jing G C. (1999): Preliminary research on the main form character of ravine freeze-thaw erosion in Kebai black soil region. Scientific and Technical Information of Soil and Water Conservation, 1: 28–30. (in Chinese)

Mi W.J., Zhang F., Jia Y., Ding F.L., Zhang X.B., Fang Z.H., Sun M.H. (2021): Slope aspect difference in slope green plant protection in Ningxia section of Yinchuan-Xi'an high-speed railway. Journal of Railway Engineering Society, 9: 87–92. (in Chinese)

Oparaku L.A., Iwar R.T. (2018): Relationships between average gully depths and widths on geological sediments

https://doi.org/10.17221/106/2021-SWR

underlying the Idah-Ankpa Plateau of the North Central Nigeria. International Soil and Water Conservation Research, 6: 43–50.

Pan M.H., Wu Y.Q., Ren F.P. (2012): Estimating soil erosion in the Dongjiang river basin based on USLE. Journal of Natural Resources, 25: 2154–2164. (in Chinese)

Poesen J., Nachtergaele J., Verstraeten G., Valentin C. (2003): Gully erosion and environmental change: importance and research needs. Catena, 50: 91–133.

Ranzi R., Le T.H., Rulli M.C. (2012): A RUSLE approach to model suspended sediment load in the to river (Vietnam): Effects of reservoirs and land use changes. Journal of Hydrology, 422: 17–29.

Rawat K.S., Mishra A.K., Bhattacharyya R. (2016): Soil erosion risk assessment and spatial mapping using LANDSAT-7 ETM+, RUSLE, and GIS-a case study. Arabian Journal of Geosciences, 9: 1–22.

Renard K.G., Foster G.R., Weesies G.A., Mccool D.K., Yoder D.C. (1997): Predicting soil erosion by water: a guide to conservation planning with the Revised Universal Soil Loss Equation (RUSLE). Agricultural Handbook, 702: 107.

Seutloali K.E., Beckedahl H.R., Dube T., Sibanda M. (2016): An assessment of gully erosion along major armoured roads in south-eastern region of South Africa: A remote sensing and GIS approach. Geocarto International, 31: 225–239.

Shen B., Fan J.R., Pan Q.B., Hui L.J. (2003): The situation of comprehensive prevention and control pilot project of soil erosion in Black Soil Area of Northeast China. Soil and Water Conservation in China, 11: 7–8. (in Chinese)

Shirazi M.A., Boersma L. (1984): A unifying quantitative analysis of soil texture. Soil Science society of America Journal, 48: 142–147.

Song X.F., Duan Z., Niu H.S., Yasuyuki K. (2009): Estimation of the cover and management factor for modeling soil erosion using remote sensing. Journal of Beijing Forestry University, 31: 58–63. (in Chinese)

Thampapillai D.J., Anderson J.R. (1994): A review of the socio-economic analysis of soil degradation problems for developed and developing countries. Review of Marketing & Agricultural Economics, 62: 291–315.

Wang D.C., Fan H.M. (2019): Distribution characteristics of gullies with slope gradient in Northeast China. Environmental Monitoring and Assessment, 191: 379.

Wang D.C., Fan H.M., Fan X.G. (2017): Distributions of recent gullies on hillslopes with different slopes and aspects in the black soil region of Northeast China. Environmental Monitoring and Assessment, 189: 508.

Wang P., Ding Z. Q., Hua H.L., Li Y.H., Duan X. (2021): Geomorphological characteristics and their impacts on land use. Patterns in Laoshan Nature Reserve of Yunnan Province. Bulletin of Soil and Water Conservation, 41: 287–295. (in Chinese)

Wang W.J., Zhang S.W., Fang H.Y. (2012): Coupling mechanism of slope-gully erosion in typical black soil area of Northeast China. Journal of Natural Resources, 27: 2113–2122. (in Chinese)

Wang W.J., Deng R.X., Zhang S.W. (2014): Preliminary research on risk evaluation of gully erosion in typical black soil area of Northeast China. Journal of Natural Resources, 29: 2058–2067. (in Chinese)

Wu Y.Q., Zheng Q.H., Zhang Y.G., Liu B.Y., Cheng H., Wang Y.Z. (2008): Development of gullies and sediment production in the black soil region of Northeastern China. Geomorphology, 101: 683–691.

Xia L., Song X.Y., Fu N., Meng C.F., Li H.Y., Li Y.L. (2017): Impacts of precipitation variation and soil and water conservation measures on runoff and sediment yield in the Loess Plateau Gully Region, China. Journal of Mountain Science, 14: 2028–2041.

Xu Y.Q., Shao X.M., Kong X.B., Peng J., Cai Y.L. (2008): Adapting the RUSLE and GIS to model soil erosion risk in a mountains karst watershed, Guizhou Province, China. Environmental Monitoring and Assessment, 141: 275–286.

Yan Y.C., Zhang S.W., Li X.Y., Yue S.P. (2005): Temporal and spatial variation of erosion gullies in Kebai Black Soil Region of Heilongjiang during the past 50 years. Scientia Geographica Sinica, 60: 1015–1020. (in Chinese)

Yan Y.C., Zhang S.W., Yue S.P. (2006): Application of corona and spot imagery on erosion gully research in typical black soil regions of Northeast China. Resources Science, 28: 154–160. (in Chinese)

Yan Y.C., Zhang S.P., Yue S.P. (2007): Classification of erosion gullies by remote sensing and spatial pattern analysis in black soil region of Eastern Kebai. Scientia Geographica Sinica, 27: 193–199. (in Chinese)

Yang D.L., Wang Z.C., Hu W.M., Cao D., Liu H. (2020): Survey of remote sensing image information extraction methods in rocky desertification areas. Safety and Environmental Engineering, 27: 137–145. (in Chinese)

Yang Q.K., Guo W.L., Zhang H.M., Wang L., Cheng L., Li J. (2010): Method of extracting LS factor at watershed scale based on DEM. Bulletin of Soil and Water Conservation, 30: 203–206 + 211. (in Chinese)

Yu X.J., Wei Y.M. (2010): Study on soil erosion characters in different slopes. Research of Soil and Water Conservation, 17: 103–106. (in Chinese)

Yuan L.F., Yang G.S., Zhang Q.F., Li H.P. (2016): Soil erosion assessment of the Poyang lake basin, China: Using USLE, GIS and remote sensing. Journal of Remote Sensing & GIS, 5: 2469–4134.

https://doi.org/10.17221/106/2021-SWR

Zhang H.M., Yang Qi. K., Li R., Liu Q.R. (2012): Research on the estimation of slope length in distributed watershed erosion. Journal of Hydraulic Engineering, 43: 437–444. (in Chinese)

Zhang K.L., Peng W.Y., Yang H.L. (2007): Soil erodibility and its estimation for agricultural soil in China. Acta Pedologica Sinica, 44: 7–13. (in Chinese)

Zhang T., Liu G., Duan X., Wilson G.V. (2016): Spatial distribution and morphologic characteristics of gullies in the Black Soil Region of Northeast China: Hebei watershed. Physical Geography, 37: 228–250.

Zhang W.B., Xie Y., Liu B.Y. (2002): Rainfall erosivity estimation using daily rainfall amounts. Scientia Geographica Sinica, 22: 705–711. (in Chinese)

Zhang X.H., Hou W.Z, Wang N. (2006): C-value in the model of soil erosion in black earth area in the Northeastern China. Journal of Agro-Environment Science, 25: 797–801. (in Chinese)

Zhang X.K., Xu J.H., Lu X.Q., Deng Y.J. (1992): A study on the equation in Heilongjiang Province. Bulletin of Soil and Water Conservation, 12: 1–10.

Zhang Y.G., Wu Y.Q., Liu B.Y., Zheng Q.H., Yin J.Y. (2007): Characteristics and factors controlling the development of ephemeral gullies in cultivated catchments of black soil region, Northeast China. Soil & Tillage Research, 96: 28–41.

Zhang Y., Wu Y.H., Zhang J.Q., Hang R., Zhao F. (2021): Effects of slope aspects on soil nutrient characteristics at rain-fed ecological experiment demonstration site in Lanzhou. GrasslandandTurf, 41: 87–92. (in Chinese)

Received: July 25, 2021
Accepted: February 4, 2022
Published online: February 28, 2022